HHS Public Access

Author manuscript

J Med Chem. Author manuscript; available in PMC 2017 November 09.

Published in final edited form as:

J Med Chem. 2017 March 09; 60(5): 1665–1672. doi:10.1021/acs.jmedchem.6b01483.

Nonclassical Size Dependence of Permeation Defines Bounds for Passive Adsorption of Large Drug Molecules

Cameron R. Pye[†,iD], **William M. Hewitt**[†,iD], **Joshua Schwochert**[†], **Terra D. Haddad**[†], **Chad E. Townsend**[†], **Lyns Etienne**[†], **Yongtong Lao**[†], **Chris Limberakis**[‡], **Akihiro Furukawa**[⊥], **Alan M. Mathiowetz**[§], **David A. Price**[§], **Spiros Liras**[§], and **R. Scott Lokey**[*,†,iD]

[†]Department of Chemistry and Biochemistry, University of California, Santa Cruz, California 95064, United States

[‡]World Wide Medicinal Chemistry, Groton Laboratories, Pfizer Inc., Groton, Connecticut 06340, United States

[§]World Wide Medicinal Chemistry, Cambridge Laboratories, Pfizer Inc., Cambridge, Massachusetts 02139, United States

[⊥]Modality Research Laboratories, Daiichi Sankyo Co., Ltd., 1-2-58 Hiromachi, Shinagawa-ku, Tokyo 140-8710, Japan

Abstract

Macrocyclic peptides are considered large enough to inhibit “undruggable” targets, but the design of passively cell-permeable molecules in this space remains a challenge due to the poorly understood role of molecular size on passive membrane permeability. Using split-pool combinatorial synthesis, we constructed a library of cyclic, per-N-methlyated peptides spanning a wide range of calculated lipohilicities ($0 < A\log P < 8$) and molecular weights (~800 Da < MW < ~1200 Da). Analysis by the parallel artificial membrane permeability assay revealed a steep drop-off in apparent passive permeability with increasing size in stark disagreement with current permeation models. This observation, corroborated by a set of natural products, helps define criteria for achieving permeability in larger molecular size regimes and suggests an operational cutoff, beyond which passive permeability is constrained by a sharply increasing penalty on membrane permeation.

[*]**Corresponding Author**. slokey@ucsc.edu; phone: 831-459-1307.

ORCID

Cameron R. Pye: http://orcid.org/0000-0002-4122-2078

William M. Hewitt: http://orcid.org/0000-0002-2881-7704

R. Scott Lokey: http://orcid.org/0000-0001-9891-1248

ASSOCIATED CONTENT

Supporting Information

The Supporting Information is available free of charge on the http://pubs.acs.org at DOI: http://pubs.acs.org/doi/abs/10.1021/acs.jmedchem.6b01483.

Detailed experimental procedures, additional data for the compounds studied herein, as well as characterization of the pure compounds (http://pubs.acs.org/doi/suppl/10.1021/acs.jmedchem.6b01483/suppl_file/jm6b01483_si_001.pdf)

Molecular formula strings (http://pubs.acs.org/doi/suppl/10.1021/acs.jmedchem.6b01483/suppl_file/jm6b01483_si_002.csv)

The authors declare no competing financial interest.

Graphical abstract

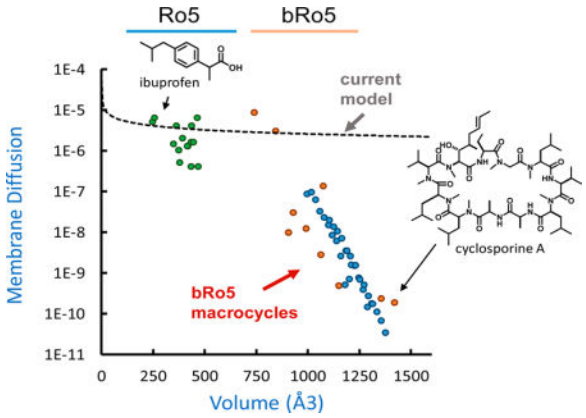

INTRODUCTION

Predicting membrane permeability is a key challenge in medicinal chemistry, as diffusion across membranes is required for orally delivered drugs and for drugs with intracellular targets. In modern medicinal chemistry, the “drug-likeness” of a compound is often evaluated by comparing its properties to those of a historical training set of drugs, giving rise to knowledge-based structure–property relationships to help guide the design of drugs with favorable properties. These quantitative (and qualitative) models include Lipinski’s Rule of 5 (Ro5), which provides a simple metric for predicting ADME properties based on molecular weight (MW), number of hydrogen bond donors and acceptors, and octanol–water partition coefficient (LogP).[1] Compounds that do not follow Lipinski’s rules are more likely to be rejected from screening collections or eliminated from consideration in medicinal chemistry campaigns, thus reinforcing the criteria and potentially hindering exploration outside this well-defined chemical space. Indeed, there are a number of notable outliers that challenge the wisdom of a strict adherence to these ADME rules. Particularly noteworthy are compounds with molecular weights above 1000 Da that show significant passive membrane permeability and, in some cases, oral bioavailability.[2] Of these rule-breaking molecules, some are macrocyclic natural products such as the cyclic peptide cyclosporine A (CSA), a 1202 Da compound that is cell permeable by passive diffusion and has an oral bioavailability of 28%. Outliers such as CSA suggest that compounds outside the Rule of 5 are able to exhibit favorable ADME properties and that potentially vast regions of chemical space remain underutilized. Recent work has focused on the classification of these “beyond Rule of 5” (bRo5) compounds using QSPR techniques based on calculable molecular properties that often belie their physical underpinnings.[3,2,4] The question remains to what extent CSA and similar compounds are true outliers, or whether they point toward untapped chemical potential and the prospect of designing permeable molecules with molecular weights well outside conventional boundaries.

There is an extensive body of literature on the physics of passive membrane permeability dating back to the solubility diffusion theory (eq 1) proposed by Overton in the 19th century.[5] This model treats the membrane as a thin slab of hydrocarbon solvent in which the

rate of membrane permeation (the permeability coefficient P_m) is equal to the hydrocarbon/water partition coefficient $K_{hc/w}$ times the membrane diffusion coefficient D divided by the membrane thickness (δ)

$$P_m = \frac{K_{hc/w} D}{\delta} \quad (1)$$

$$D = \frac{k_B T}{6\pi\eta r} \quad (2)$$

This models only form of size dependence is the diffusion term, which has been approximated by the Stokes–Einstein equation (eq 2) and is dependent on the radius of the solute (r), the viscosity of the medium (η), and the temperature (T). However, this diffusion term alone does not accurately capture the observed size dependence on permeability even within Ro5 space. More recent models have attempted to address this discrepancy by asserting that diffusion through the ordered membrane more closely resembles the diffusion of solutes in polymers.[6] In polymer-type diffusion, the solute migrates through the medium by traversing a series of stochastically appearing holes that are of greater volume than that of the compound. Extending this principle, Xiang and Anderson proposed that there was an additional penalty associated with a lateral pressure that must be overcome during partitioning into the membrane to create a cavity of sufficient volume to accommodate the solute.[7,8] Recently, implementations of these models have been successfully applied to the prediction of permeabilities for compounds in the “extended Ro5” size range (500–850 Da) but have yet to successfully predict the permeability of compounds approaching the MW of CSA.[9,10]

Only a handful of natural products and, more recently, synthetic cyclic peptides, have been described with molecular weights above ~1000 that show bone fide passive membrane permeability.[11,12] This raises the question whether, or to what extent, the design rules developed for extended Ro5 compounds will apply to these significantly larger systems. Herein, we report the application of a synthetic library approach toward understanding the impact of lipophilicity and molecular size on the intrinsic permeability of peptidic macrocycles in the size range of CSA and similar natural products. We designed a library of cyclic peptides with MW > ~800 and assayed their permeabilities to elucidate the size dependence of permeability in this space. All compounds were permethylated at the backbone to eliminate intramolecular hydrogen bonding (IMHB) and the resulting conformational effects as potentially complicating factors. After accounting for aqueous solubility and using experimentally determined hydrocarbon–water partition coefficients, we observed a steep, unprecedented size penalty for increasing molecular size in the bRo5 space that is no accounted for using current physics-based or QSPR models of permeability.

RESULTS

Aggregation Imposes a Limit on Apparent Permeability

To quantify permeability over a wide range of sizes and lipophilicities, we synthesized a split pool library of hydrophobic octapeptides that spanned a MW range from 784 to 938 (Figure 1A). All library members contained a Tyr residue for linkage to the resin via the side chain phenol as well as a D-Pro residue to facilitate cyclization. The additional residues were comprised of combinations of Ala, Leu, and Ile. All of the library members had the same backbone stereochemistry arising from a previous, unpublished scaffold whose high predicted permeability was compromised by poor solubility. Finally, all of the scaffolds were permethylated before cleavage from solid support. Complete *N*-methylation was designed to eliminate the possibility of intramolecular hydrogen bonding in the backbone, thus providing a controlled model system for evaluating the impact of size and lipophilicity independent of backbone conformation. A separate library was synthesized in tandem using Ile in place of Leu to test whether the shape of the alkyl side chains impact any observed permeability trends.

The parallel artificial membrane permeability assay (PAMPA) is a model of membrane permeability that is widely used as a cell-free system for measuring passive permeability and has been shown to correlate with in vivo oral bioavailability.[13,14] PAMPA allows for the assessment of a compound's passive membrane permeability without convoluting factors such as paracellular diffusion and active efflux and transport mechanisms present in cell-based models. We have previously shown that the assay can be multiplexed using LC-MS to enable simultaneous quantification and deconvolution of complex mixtures.[15] Using this methodology, we discovered several novel cyclic hexapeptides with good to excellent membrane permeabilities. Both the Leu/Ala and Ile/Ala libraries were assayed using this multiplexed PAMPA assay to evaluate the permeability of all library species. Only compounds comprised of two Ala and four Xaa residues (Xaa = Leu or Ile) showed appreciable permeability (Figure 1b). This result suggested that there is an optimal lipophilicity window in which significant permeability can be achieved within this system. We selected individual compounds from the library for synthesis and assayed their permeabilities in PAMPA as well as a cell-based permeability assay using a low-efflux MDCK cell line in which P-glycoprotein expression has been reduced (MDCKII-LE).[16] Although the magnitudes of the permeabilities for the individual compounds were higher, the trends observed in the libraries were in good agreement with the trends observed in the assay of mixtures, demonstrating that the trend was not an artifact of the multiplexed in vitro assay and that the observed permeabilities correlated with composition irrespective of the specific sequences (Figure S1).

Lipophilicity Scanning Library

To more thoroughly investigate the combined effect of lipophilicity and MW on permeability, we designed a combinatorial library of permethylated octa-, nona-, and decapeptides. As in the previous library, each member contained a Tyr and Pro residue, and the variable positions were populated with a combination of simple, straight chain aliphatic residues: Ala, aminobutyric acid (Abu), norvaline (Nva), and norleucine (Nle) (Figure 2).

The library was designed to span a wide range of molecular weights (797–1237) and lipophilicities ($0 < A\log P < 8$) with compositional isomers that sampled lipophilicities in increments of one -CH_2-group corresponding to 0.4 log units of AlogP. The octa-, nona-, and decapeptide libraries were analyzed separately. Permeabilities were determined for all -CH_2- (i.e., $A\log P$) increments, which eluted separately on a reverse phase (C18) HPLC gradient ($H_2O \rightarrow$ ACN) and were thus evaluated as groups of constitutional isomers (Figure 3a). As ring size increased, the overall permeabilities decreased, even among compounds in the same $A\log P$ range. This general inverse correlation between MW and permeability has been observed previously for small sets of low-MW compounds.[17] However, we could not determine whether the magnitude of the MW penalty observed in our system was consistent with current models. In addition, we observed a bilinear relationship between permeability and lipophilicity. This decrease in apparent permeability beyond $A\log P \approx 4.5$ has been reported for other model systems and is consistent with knowledge-based models such as the Rule of 5 and others that place an upper limit on lipophilicity.[18–20] However, there is a lack of consensus as to whether this decrease in permeability at higher $A\log P$ values is due to poor solubility or sequestration into the PAMPA membrane, and the phenomenon may depend on the particular system involved.[20,21]

In contrast to $A\log P$, which is a calculated descriptor based on octanol/water partition coefficients, experimental partition coefficients between water and hydrocarbon solvents such as 1,9-decadiene have been shown to provide a good correlation with experimental permeabilities in physics-based permeability models.[22] Octanol can form hydrogen bonds with solute and therefore provides a poor model for the desolvation of highly polar groups such as hydrogen bond donors.[23] However, in a series of homologous compounds that differ only by hydrocarbon chain lengths, a high correlation is observed between octanol/water and hydrocarbon/water partition coefficients.[23] To determine whether the apparent permeabilities observed in our system are concordant with current physics-based models, we set out to (1) determine their hydrocarbon/water partition coefficients experimentally and (2) account for the decrease in solubility at higher lipophilicities to determine their intrinsic permeabilities.

We selected 1,9-decadiene as the hydrocarbon solvent for shake-flask partition coefficient measurements ($SF\log K_{hc/w}$) because it had been reported to give the best correlation to experimental permeabilities.[7] We found a very good linear fit over ~5 log units between experimental 1,9-decadiene/buffer partition coefficients and $A\log P$ (Figure 3b), suggesting that partitioning into hydrocarbon in this system is dominated by the aliphatic side chains and that conformational effects (e.g., by way of steric shielding) are either small or similar for all library members. A linear regression was used to extrapolate $\log K_{hc/w}$ values for compounds that were below the detection limits of the instrument in either of the two phases. The MDCK-LE permeabilities for individual compounds were measured and compared to their permeabilities in the PAMPA system (Figure 3c). The linearity of the data suggests that the PAMPA assay is correlated with the more biologically relevant cell-based assay, while the lower values in PAMPA vs MDCK may be related to differences in membrane retention between the two systems.[24]

Solubility Adjustment via Filtration

The solvent-diffusion model predicts a linear relationship between the log of intrinsic permeability ($\log P_0$) and membrane partition coefficient ($\log K_{mem}$) with unit slope, and this behavior has been observed for a variety of compounds, including small linear peptides.[25,26] At higher lipophilicities, our cyclic peptides deviate substantially from this expected linear relationship, prompting us to test whether this decrease in apparent permeability could be attributed to a decrease in water solubility at the higher $\log K_{hc/w}$ values (Figure 4A).

Apparent permeability coefficients (P_{app}) are typically calculated based on the assumption that the concentration of compound added to the donor compartment (in practice, usually ~10 μM) represents the solution concentration of the permeable species in the assay. To determine intrinsic permeabilities (P_0), we used a filtration solubility assay to determine the concentration of soluble monomeric (or small <200 nm oligomeric) compound for each $A\log P$ (or SF$\log K_{hc/w}$) increment. Solutions were prepared using the same concentration and buffer conditions as those used in the permeability assay. The solutions were then filtered through 0.2 μm nylon filters so that only very small aggregates or monomeric species could pass through and then quantitated by LC/MS using samples dissolved in MeOH as standards. The buffer-to-MeOH intensity ratios for each group of isomers thus provided a "solubility decrement" factor for adjusting P_{app} values based on true solubilities. Above $\log K_{hc/w} \approx -1$, solubilities fell off precipitously as a function of $\log K_{hc/w}$ (Figure 4a–c).

Analogous to the adjustment commonly applied to permeants with ionizable groups, we adjusted the P_{app} value by the soluble fraction available (f_{sol}) using eq 3.[27] When we applied this solubility adjustment to P_{app}, we observed a linear relationship as predicted by models relating intrinsic permeability P_0 to $K_{hc/w}$ as indicated in Figure 4 by the regression lines (orange markers). Although linearity is observed (consistent with a linear free energy relationship between partition coefficients and membrane transport rates), the slope is notably less than 1 (0.47, 0.48, 0.53 for the octa-, nona-, and deca- libraries, respectively). This suggests that the increase in P_0 with increasing lipophilicity is not fully explained by the corresponding change in $K_{hc/w}$.

$$\frac{1}{P_{app}} = \frac{1}{P_0 * f_{sol}} \quad (3)$$

Nonclassical Diffusion of bRo5 Compounds

Despite the linear relationship between $\log K_{hc/w}$ and $\log P_0$, the slope was significantly less than 1, and the intercepts decreased with increasing ring size, suggesting that there is an additional permeability penalty not accounted for with the solubility adjustment. The solubility-diffusion model has served as the basis for more modern treatments predicting the role of size in membrane diffusion (e.g., the barrier-domain model).[7,10,28] To compare scaffolds of different lipophilicities and sizes, one can solve eq 1 for the apparent membrane diffusion term D_{mem} to obtain the following

$$D_{\mathrm{mem}} = \frac{P_0 * \delta}{K_{\mathrm{mem}}} \quad (4)$$

where P_0 is our solubility-adjusted P_{app}, K_{mem} is the $K_{\mathrm{hc/w}}$ value from the 1,9-decadiene partition experiments, and δ is the thickness of the membrane in cm. Using a reported thickness 0.125 cm, we plotted diffusions of compounds across the PAMPA membrane.[29] It should be noted that solving for D_{mem} in the solubility diffusion equation is not necessarily evidence for a diffusion-mediated mechanism. The size dependence may arise from a combination of factors including partitioning penalties.[7] Plotting the apparent membrane diffusion of small molecules (using published experimental $\log K_{\mathrm{hc/w}}$ and $\log P_0$ values[30]) versus their McGowan volume[31] reveals a roughly exponential relationship that follows the same form as Stokes–Einstein diffusion (Figure 5, black broken line). However, with our library compounds, we find a steep drop-off beginning at a molecular volume of ~1000 Å^3 (corresponding to a MW of ~1000 Da) that deviates from the exponential approximation (Figure 5, blue points).

Extension to Other Scaffolds

To ensure that this trend was not particular to the macrocyclic scaffolds used in our study, we selected a variety of commercially available or synthetically tractable cyclic peptide natural products in this size range that we anticipated could be passively permeable. This diverse set of compounds allowed us to extend our observations beyond the permethylated model system to scaffolds that are potentially more relevant in a drug discovery context. Using the panel of assays described above, we determined their apparent D_{mem} values (Figure 5, orange markers). These data followed the same sharp downward trend above a volume of ~1000 Å^3 (MW ≈ 975) that was seen for the octa-, nona-, and decapeptides described above. The sharp decrease in $\log D_{\mathrm{mem}}$ observed in this MW range is not predicted by models with molecular volume dependencies, either in the diffusion term (V^{-n}) or in the partition term ($\exp[-V^n]$) (or a combination of both).[28,17,7]

Generalizing these results, the $\log K_{\mathrm{hc/w}}$ required to achieve the generally accepted minimum threshold for permeability of $P_{\mathrm{app}} = 1 \times 10^{-6}$ cm/s can be approximated at a given molecular volume (Figure 6). As volume increases, the $\log K_{\mathrm{hc/w}}$ required to overcome the size penalty is so great that aqueous solubility begins to rapidly decline. In practice, this applies an upper limit on the size of compounds that are likely to be passively permeable and confines large molecular weight scaffolds to a narrow lipophilicity window (green shaded area). These large compounds must have lipophilicities that are high enough to overcome the steep size dependence observed but low enough to maintain reasonable aqueous solubility. It should be noted that the relationship observed in our system between molecular size and intrinsic permeability is in agreement with the observation by Doak et al. that very few orally delivered drugs exist beyond MW ≈ 1000.[2]

DISCUSSION AND CONCLUSIONS

In this work, we set out to investigate the relationship between lipophilicity, size, and membrane permeability in a molecular weight range yet to be thoroughly interrogated. By using splitpool combinatorial syntheses and multiplexed assays, we were able to evaluate thousands of compounds displaying a wide range of sizes and lipophilicities. The use of permethylated amide backbones and straight chain alkyl side chains allowed us to probe compositional trends without convoluting factors arising from intramolecular hydrogen bonding and associated conformational effects. Physical models that describe permeability refer to the intrinsic permeability (P_0) as opposed to the experimentally observed apparent permeability (P_{app}), which can make comparison to experimental values difficult.

Notably, the slopes of the relationships between $\log P_0$ and $\log K_{hc/w}$ were less than unity, indicating that the incremental increase in $\log K_{hc/w}$ for each additional -CH_2- group corresponds to a smaller relative increase in $\log P_0$. Given that molecular size also increases with lipophilicity in these plots, the deviation from unity is consistent with a strong size dependence on permeability. By adjusting our experimental P_{app} for solubility, we were able to compare P_0 values with other published data sets. Solving the general permeability equation (eq 1) for the size-dependent diffusion term, we discovered a steep size dependence for compounds with volumes in the bRo5 molecular weight range. With the current dataset, we can only speculate about the mechanistic origin of this size dependence. It appears that there could be more than one rate limiting step for the permeation of these large hydrophobic macrocycles. It is clear from Figure 5 that Stokes–Einstein diffusion cannot account for the size dependence observed, but other more restrictive diffusion schemes akin to the diffusion of solutes through polymeric matrices might be at play as has been suggested by others.[6] Additionally, increased resolvation penalties associated with departitioning from the membrane may cause membrane exit to become an additional rate limiting step.[32]

The model compounds presented here, permethylated species with only one hydrogen bond donor and the phenolic hydroxyl, are not necessarily representative of many bRo5 compounds that contain multiple hydrogen bond donors, where conformational effects may be much more important. Polar groups in the backbone of therapeutically relevant macrocycles have been shown to be important for protein target binding,[4] and the ability to adopt lipophilic conformations is required to mitigate the deleterious effect of these polar groups on permeability. The low dielectric conformation that CSA adopts in the membrane substantially decreases the desolvation cost of partitioning and might minimize the effective radius, allowing CSA not only to “smuggle” polar backbone groups into the cell but also to do so in a conformation that minimizes the cavity size needed to accommodate it.[25] These 3D effects of conformation are not captured in the simple 2D molecular volume used in plotting D_{mem}, which may be why CSA lies to the right of the regression line in Figure 5. Previous studies on the effect of size on permeability have used the 3D radius of gyration descriptor; this descriptor requires knowledge of the conformational landscape, which is difficult to determine for large ring systems described in this paper and as such is not used.[3] However, the separate set of diverse compounds (Figure 5, orange points) containing hydrogen bond donors (and conformation-dependent properties) followed roughly the same

sharp decline in membrane diffusion as our model compounds when using the thermodynamic solubility adjustments and equilibrium SFlog$K_{hc/w}$ values, suggesting that the observed size dependence is not particular to scaffolds that lack conformational effects. It should be noted that these compounds are also cyclic peptide species (structures and characterization provided in Supporting Information), and though their chemical nature is substantially more diverse than the library described herein, the generality of these trends has yet to be thoroughly investigated with nonpeptidic compounds in this space.

Predicting precise values of P_0 ab initio for a diverse set of molecules is a difficult task that requires knowledge of the molecules' conformational states as well as the composition of the membrane in question. However, the bulk physical properties that contribute to the intrinsic permeability are relatively simple: K_{mem} (approximated as $K_{hc/w}$) and size (approximated as ~MW). In contrast to intrinsic permeability (P_0), apparent permeability (P_{app}) depends on additional factors that must be considered, including the aqueous boundary layer, pK_a, and aqueous solubility. Even the most permeable species in this range are well below the aqueous boundary threshold (~10^{-4} cm/s), leaving solubility and pK_a as the main factors to consider aside from size and lipophilicity when assessing the potential apparent permeability of bRo5 molecules. For achieving K_{mem} values that are high enough to offset the intrinsic size penalty in bRo5 space, any ionizable groups are likely to be prohibitively deleterious. The fraction of available compound depends on both solubility and pK_a, and if a large compound is not fully soluble at the required lipophilicity to permeate, the addition of an ionizable group, although it may substantially increase the soluble fraction, will likely prohibitively decrease K_{mem}. However, in principle, a balance could be achieved with the incorporation of solubilizing groups (e.g., morpholine or other tertiary amines) whose pK_a values are close to neutral. It has been shown in previous studies that conformational flexibility can help improve solubility of bRo5 macrocyclic compounds in some cases, though the exact mechanism by which the "chameleonicity" gives rise to these desirable properties is still poorly understood.[33–35] Poor aqueous solubility can also be alleviated (to a point) by modern pharmaceutical formulation chemistry. The use of nm-scale dispersions and other solubility-enhancing delivery systems such as emulsifiers and liposomes can greatly improve the oral bioavailability of highly lipophilic drugs.[36]

Cyclic peptides and peptide-containing macrocycles have received a lot of attention due to their synthetic tractability and a renewed enthusiasm for their potential to exhibit druglike pharmacokinetic properties.[37] Although a variety of combinatorial strategies (DNA-encoded, mRNA display, phage display libraries, etc.) have been developed that can yield macrocycles with potencies that rival those of antibodies, they tend to produce molecules with multiple polar side chains. Although these residues can be critical for high affinity, they can virtually eliminate the possibility for passive cell permeability.[38,39] There are other modalities that can be employed to effect cell permeability that rely on various nonpassive or pseudopassive mechanisms (e.g., micropintocytosis, membrane disruption, possibly other uncharacterized transport pathways).[40–42] For example, charge-mediated transport mechanisms employed by incorporating a series of cationic residues have been demonstrated to overcome the passive permeability problems by bypassing the mechanism altogether.[43] However, although these strategies have been effective in cell culture and even in animals,[42] there are still no compounds in this class that have progressed through clinical trials, perhaps

due to the complexities associated with cation-mediated transport in the varied cell types found in biological tissues. Despite the severe constraints placed on molecular volume by conventional, passive membrane diffusion, the permeable chemical space between MW 500 and 1000 remains virtually untapped. Nature has provided us with a diverse set of examples that manage to walk the line between permeability and solubility. In addition to CSA, scaffolds with very different structures such as cylindrocyclin and patellamide C have druglike passive permeabilities.[27] Although the challenge of achieving both permeability and solubility increases sharply beyond the Rule of 5, so does the number of synthetically accessible scaffolds. Mining this chemical space for compounds of therapeutic value will be a challenging but lucrative endeavor of this field for decades to come.

EXPERIMENTAL SECTION

General

All chemicals were commercially available and used without further purification. For reverse-phase column chromatography, a SNAP C18 cartridge (30 g, Biotage) was employed. NMR spectra were recorded in $CDCl_3$, Pyridien-d_5, or DMSO-d_6 (depending on solubility) on a Varian 500 MHz NMR instrument with Unity Plus console and 5 mm broad-band probe at 25 °C. Chemical shifts were referenced to residual solvent proton signals. The purities of individual compounds were tested by HPLC (Waters 1525) with an attached mass spectrometer (Micromass ZQ, waters) and PDA detector (Waters 2998) through a 3.5 μm C18 column (XBridge BEH C18 4.6 × 50 mm). The mixture of water (0.1% formic acid) and ACN (0.1% formic acid) was used as an eluent, of which ACN percentage was increased stepwise (0–2 min, 20%; 2–10 min, linear gradient from 20 to 100%; 10–12 min, 100%) with a flow rate of 1.2 mL/min. Pure, diverse compounds were analyzed on the same instrument and solvent system using a Thermo Accucore C18 column (50 × 4.6 mm) with 2.6 μm packing material. The ACN was again increased stepwise (0–1 min, 20%; 2–10 min, linear gradient from 20 to 100%; 2–4 min, 100%) with a flow rate of 1.9 mL/min. The absorbance at 220 nm wavelength was used to calculate the purity, and all individual compounds were at least 95% pure. LC-MS analyses for PAMPA were performed on a UHPLC (UltiMate 3000, Dionex) with an attached mass spectrometer (Orbitrap Velos Pro, Thermo Scientific) through a 1.9 μm C18 column (Hypersil GOLD 30 × 2.1 mm, Thermo Scientific). The mixture of water (0.1% formic acid) and ACN (0.1% formic acid) was used as an eluent using a short trap, and the elute method ACN was held at an initial value of 10% for 1 min followed by a rapid linear gradient (30 s) to 95%, which was held for 1.75 min before returning to starting column conditions with a flow rate of 1 mL/min.

Cyclic Peptide Synthesis

Permethylated peptides were synthesized on Fmoc-tyrosine-OAllyl 2-chlorotrityl resin (0.3–0.5 mmol/g) loaded through the side chain phenol. Couplings were performed using standard Fmoc coupling conditions (Fmoc amino acid/HATU/DIPEA in DMF, 1.5 h). The linear peptides were deprotected (N-terminal Fmoc and C-terminal allyl) using a solution of $Pd(Ph_3P)_4$ and piperidine. Cyclization was performed on-resin using PyBOP/HOAt/DIPEA for 3 h in DMF. The resulting cyclic species were then permethylated by deprotonating using 3 equiv of potassium *tert*-butoxide in DMSO/THF followed by immediate treatment with

MeI (10 equiv). The library compounds were cleaved using 5% TFA in DCM, evaporated, and used as crude mixtures. Individual compounds were purified as described above. Pure compounds from the diverse compound set were synthesized using a variety of standard Fmoc-based solid phase synthesis techniques including HATU and HBTU couplings and incorporation of pre-*N*-methylated monomers. The synthetic schemes and characterization of each unique compound is detailed in the Supporting Information.

Shake Flask log$K_{hc/w}$ Assay

Reagent-grade 1,9-decadiene was saturated with H_2O prior to use. One microliter of ~10 mM DMSO stock was transferred to 1 mL of 1,9-decadiene/$H_2$0 (1:1). After thorough agitation, the system was allowed to reach equilibrium overnight. Then, 100 μL aliquots of each phase were taken and evaporated under a stream of air. Each aliquot was then suspended in MeOH and quantified via LC-MS.

Filtration Solubility

Filtration solubility samples were prepared by transferring 10 μL of ~10 mM DMSO stock solution to 990 μL of PBS (pH 7.4). The solution was vortexed and allowed to reach the thermodynamic solubility product overnight. The solution was then centrifuged at 16000*g* for 5 min, and the supernatant was then filtered through a 0.2 μm syringe-driven filter. The first half of the filtrate (~0.5 mL) was discarded, and the second half was quantified via LCMS. A reference solution was prepared by diluting 10 μL of the same DMSO stock into MeOH and quantified immediately after preparation via LC-MS.

PAMPA

The PAMPA assay was run using a 96-well filter plate with 0.45 μm hydrophobic Immobilon-P membrane supports (Millipore). Five microliters of 1% lecithin in *n*-dodecane was applied to the filter to serve as the artificial membrane. Library mixtures or individual compounds were prepared from DMSO stocks diluted in PBS to a final concentration of 5% DMSO and ~10 μM. The filter donor plate was then placed into the acceptor plate, which contained 300 μL of 5% DMSO PBS and was allowed to incubate for 14 h at 25 °C in triplicate. After the incubation, the donor and acceptor plates were separated, and the concentration of each compound in the donor and acceptor wells was quantified by LC-MS to calculate P_{app}.

ALogP Calculations

*A*Log*P* values were calculated using the method described by Ghose et al.[44]

Supplementary Material

Refer to Web version on PubMed Central for supplementary material.

ABBREVIATIONS USED

ACN acetonitrile

COMU	(1-cyano-2-ethoxy-2-oxoethylidenaminooxy)dimethylamino-morpholino-carbenium hexafluorophosphate
DBU	1,8-diazabicyclo[5.4.0]undec-7-ene
DCM	dichloromethane
DIAD	diisopropyl azodicarboxylate
DMF	*N,N*-dimethylformamide
DIC	diisopropylcarbodiimide
DIPEA	diisopropylethylamine
DMSO	dimethyl sulfoxide
DVB	divinylbenzene
EtOH	ethanol
Fmoc	9-fluorenylmethoxycarbonyl
HBTU	*N,N,N′,N′*-tetramethyl-*O*-(1*H*-benzotriazol-1-yl)uronium hexafluorophosphate
HOAt	1-hydroxy-7-azabenzotriazole
IR	infrared
LC-MS	liquid chromatography mass spectrometry
MeOH	methanol
N_2	nitrogen
NMP	1-methyl-2-pyrrolidinone
PAMPA	parallel artificial membrane assay
PTFE	polytetrafluoroethylene
PyBOP	(benzotriazol-1-yloxy)tripyrrolidinophosphonium hexafluorophosphate
RP	reverse phase
SPPS	solid-phase peptide synthesis
***t*-BuOH**	*tert*-butoxide
TFA	trifluoroacetic acid
THF	tetrahydrofuran.

References

1. Lipinski CA, Lombardo F, Dominy BW, Feeney PJ. Experimental and Computational Approaches to Estimate Solubility and Permeability in Drug Discovery and Development Settings. Adv. Drug Delivery Rev. 1997; 23:3–25.
2. Doak BCC, Over BB, Giordanetto F, Kihlberg J. Oral Druggable Space beyond the Rule of 5: Insights from Drugs and Clinical Candidates. Chem. Biol. 2014; 21:1115–1142. [PubMed: 25237858]
3. Guimarães CRW, Mathiowetz AM, Shalaeva M, Goetz G, Liras S. Use of 3D Properties to Characterize Beyond Rule-of-5 Property Space for Passive Permeation. J. Chem. Inf. Model. 2012; 52:882–890. [PubMed: 22394163]
4. Villar EA, Beglov D, Chennamadhavuni S, Porco JA, Kozakov D, Vajda S, Whitty A. How Proteins Bind Macrocycles. Nat. Chem. Biol. 2014; 10:723–731. [PubMed: 25038790]
5. Overton E. No Title. Vierteljahrsschr. Naturforsch. Ges. Zurich. 1899; 44:88–135.
6. Lieb WR, Stein WD. Implications of Two Different Types of Diffusion for Biological Membranes. Nature. 1971; 234:220–222. [PubMed: 4943088]
7. Xiang T-XX, Anderson BD. The Relationship between Permeant Size and Permeability in Lipid Bilayer Membranes. J. Membr. Biol. 1994; 140:111–122. [PubMed: 7932645]
8. Xiang TX, Anderson BD. Molecular Distributions in Interphases: Statistical Mechanical Theory Combined with Molecular Dynamics Simulation of a Model Lipid Bilayer. Biophys. J. 1994; 66:561–573. [PubMed: 8011890]
9. Leung SSF, Mijalkovic J, Borrelli K, Jacobson MP. Testing Physical Models of Passive Membrane Permeation. J. Chem. Inf. Model. 2012; 52:1621–1636. [PubMed: 22621168]
10. Leung SSF, Sindhikara D, Jacobson MP. Simple Predictive Models of Passive Membrane Permeability Incorporating Size-Dependent Membrane-Water Partition. J. Chem. Inf. Model. 2016; 56:924–929. [PubMed: 27135806]
11. Bockus AT, McEwen CM, Lokey RS. Form and Function in Cyclic Peptide Natural Products: A Pharmacokinetic Perspective. Curr. Top. Med. Chem. 2013; 13:821–836. [PubMed: 23578026]
12. Fouché M, Schäfer M, Berghausen J, Desrayaud S, Blatter M, Piéchon P, Dix I, Martin Garcia A, Roth H-J. Design and Development of a Cyclic Decapeptide Scaffold with Suitable Properties for Bioavailability and Oral Exposure. ChemMedChem. 2016; 11:1048–1059. [PubMed: 27154275]
13. Kansy M, Senner F, Gubernator K. Physicochemical High Throughput Screening: Parallel Artificial Membrane Permeation Assay in the Description of Passive Absorption Processes. J. Med. Chem. 1998; 41:1007–1010. [PubMed: 9544199]
14. Testa, B.van de Waterbeemd, H.Folkers, G., Guy, R., editors. Pharmacokinetic Optimization in Drug Research. Verlag Helvetica Chimica Acta; Zürich: 2001.
15. Hewitt WM, Leung SSF, Pye CR, Ponkey AR, Bednarek M, Jacobson MP, Lokey RS. Cell-Permeable Cyclic Peptides from Synthetic Libraries Inspired by Natural Products. J. Am. Chem. Soc. 2015; 137:715–721. [PubMed: 25517352]
16. Di L, Whitney-Pickett C, Umland JP, Zhang H, Zhang X, Gebhard DF, Lai Y, Federico JJ, Davidson RE, Smith R, Reyner EL, Lee C, Feng B, Rotter C, Varma MV, Kempshall S, Fenner K, El-Kattan AF, Liston TE, Troutman MD. Development of a New Permeability Assay Using Low-Efflux MDCKII Cells. J. Pharm. Sci. 2011; 100:4974–4985. [PubMed: 21766308]
17. Nitsche JM, Kasting GB. Permeability of Fluid-Phase Phospholipid Bilayers: Assessment and Useful Correlations for Permeability Screening and Other Applications. J. Pharm. Sci. 2013; 102:2005–2032. [PubMed: 23605505]
18. Lipinski CA, Lombardo F, Dominy BW, Feeney PJ. Experimental and Computational Approaches to Estimate Solubility and Permeability in Drug Discovery and Development settings1PII of Original Article: S0169–409X(96)00423–1. The Article Was Originally Published in Advanced Drug Delivery Reviews 23 (1997) 3. Adv. Drug Delivery Rev. 2001; 46:3–26.
19. Furukawa A, Townsend CE, Schwochert J, Pye CR, Bednarek MA, Lokey RS. Passive Membrane Permeability in Cyclic Peptomer Scaffolds Is Robust to Extensive Variation in Side Chain Functionality and Backbone Geometry. J. Med. Chem. 2016; 59:9503–9512. [PubMed: 27690434]

20. Fujikawa M, Nakao K, Shimizu R, Akamatsu M. QSAR Study on Permeability of Hydrophobic Compounds with Artificial Membranes. Bioorg. Med. Chem. 2007; 15:3756–3767. [PubMed: 17418579]
21. Wang CK, Northfield SE, Swedberg JE, Colless B, Chaousis S, Price DA, Liras S, Craik DJ. Exploring Experimental and Computational Markers of Cyclic Peptides: Charting Islands of Permeability. Eur. J. Med. Chem. 2015; 97:202–213. [PubMed: 25974856]
22. Mayer PT, Anderson BD. Transport across 1,9-Decadiene Precisely Mimics the Chemical Selectivity of the Barrier Domain in Egg Lecithin Bilayers. J. Pharm. Sci. 2002; 91:640–646. [PubMed: 11920749]
23. Goodwin JT, Conradi RA, Ho NFH, Burton PS. Physicochemical Determinants of Passive Membrane Permeability: Role of Solute Hydrogen-Bonding Potential and Volume. J. Med. Chem. 2001; 44:3721–3729. [PubMed: 11606137]
24. Avdeef, A. Absorption and Drug Development. Wiley; Hoboken, NJ: 2003.
25. Mayer PT, Xiang TX, Niemi R, Anderson BD. A Hydrophobicity Scale for the Lipid Bilayer Barrier Domain from Peptide Permeabilities: Nonadditivities in Residue Contributions. Biochemistry. 2003; 42:1624–1636. [PubMed: 12578376]
26. Xiang TX, Chen J, Anderson BD. A Quantitative Model for the Dependence of Solute Permeability on Peptide and Cholesterol Content in Biomembranes. J. Membr. Biol. 2000; 177:137–148. [PubMed: 11003688]
27. Gutknecht J, Tosteson DC. Diffusion of Weak Acids across Lipid Bilayer Membranes: Effects of Chemical Reactions in the Unstirred Layers. Science. 1973; 182:1258–1261. [PubMed: 4752218]
28. Lieb WR, Stein WD. Non-Stokesian Nature of Transverse Diffusion within Human Red Cell Membranes. J. Membr. Biol. 1986; 92:111–119. [PubMed: 3761357]
29. Nielsen PE, Avdeef A. PAMPA–a Drug Absorption in Vitro Model 8. Apparent Filter Porosity and the Unstirred Water Layer. Eur. J. Pharm. Sci. 2004; 22:33–41. [PubMed: 15113581]
30. Wohnsland F, Faller B. High-Throughput Permeability pH Profile and High-Throughput Alkane/water Log P with Artificial Membranes. J. Med. Chem. 2001; 44:923–930. [PubMed: 11300874]
31. Abraham MH, McGowan JC. The Use of Characteristic Volumes to Measure Cavity Terms in Reversed Phase Liquid Chromatography. Chromatographia. 1987; 23:243–246.
32. Filipe HAL, Salvador A, Silvestre JM, Vaz WLC, Moreno MJ. Beyond Overton's Rule: Quantitative Modeling of Passive Permeation through Tight Cell Monolayers. Mol. Pharmaceutics. 2014; 11:3696–3706.
33. Whitty A, Zhong M, Viarengo L, Beglov D, Hall DR, Vajda S. Quantifying the Chameleonic Properties of Macrocycles and Other High-Molecular-Weight Drugs. Drug Discovery Today. 2016; 21:712–717. [PubMed: 26891978]
34. Bockus AT, Schwochert JA, Pye CR, Townsend CE, Sok V, Bednarek MA, Lokey RS. Going Out on a Limb: Delineating The Effects of β-Branching, N-Methylation, and Side Chain Size on the Passive Permeability, Solubility, and Flexibility of Sanguinamide A Analogues. J. Med. Chem. 2015; 58:7409–7418. [PubMed: 26308180]
35. Over B, Matsson P, Tyrchan C, Artursson P, Doak BC, Foley MA, Hilgendorf C, Johnston SE, Lee MD, Lewis RJ, McCarren P, Muncipinto G, Norinder U, Perry MWD, Duvall JR, Kihlberg J. Structural and Conformational Determinants of Macrocycle Cell Permeability. Nat. Chem. Biol. 2016; 12:1065–1074. [PubMed: 27748751]
36. Porter CJH, Trevaskis NL, Charman WN. Lipids and Lipid-Based Formulations: Optimizing the Oral Delivery of Lipophilic Drugs. Nat. Rev. Drug Discovery. 2007; 6:231–248. [PubMed: 17330072]
37. Driggers EM, Hale SP, Lee J, Terrett NK. The Exploration of Macrocycles for Drug Discovery — an Underexploited Structural Class. Nat. Rev. Drug Discovery. 2008; 7:608–624. [PubMed: 18591981]
38. Georghiou G, Kleiner RE, Pulkoski-Gross M, Liu DR, Seeliger MA. Highly Specific, Bisubstrate-Competitive Src Inhibitors from DNA-Templated Macrocycles. Nat. Chem. Biol. 2012; 8:366–374. [PubMed: 22344177]
39. Josephson K, Ricardo A, Szostak JW. mRNA Display: From Basic Principles to Macrocycle Drug Discovery. Drug Discovery Today. 2014; 19:388–399. [PubMed: 24157402]

40. Kaplan IM, Wadia JS, Dowdy SF. Cationic TAT Peptide Transduction Domain Enters Cells by Macropinocytosis. J. Controlled Release. 2005; 102:247–253.

41. Henriques ST, Huang Y-H, Chaousis S, Sani M-A, Poth AG, Separovic F, Craik DJ. The Prototypic Cyclotide Kalata B1 Has a Unique Mechanism of Entering Cells. Chem. Biol. 2015; 22:1087–1097. [PubMed: 26278183]

42. Chu Q, Moellering RE, Hilinski GJ, Kim Y, Grossmann TN, Yeh JT-H, Verdine GL, Yeh T, Verdine GL. Towards Understanding Cell Penetration by Stapled Peptides. MedChemComm. 2015; 6:111–119.

43. Trinh TB, Upadhyaya P, Qian Z, Pei D. Discovery of a Direct Ras Inhibitor by Screening a Combinatorial Library of Cell-Permeable Bicyclic Peptides. ACS Comb. Sci. 2016; 18:75–85. [PubMed: 26645887]

44. Ghose AK, Viswanadhan VN, Wendoloski JJ. Prediction of Hydrophobic (Lipophilic) Properties of Small Organic Molecules Using Fragmental Methods: An Analysis of ALOGP and CLOGP Methods. J. Phys. Chem. A. 1998; 102:3762–3772.

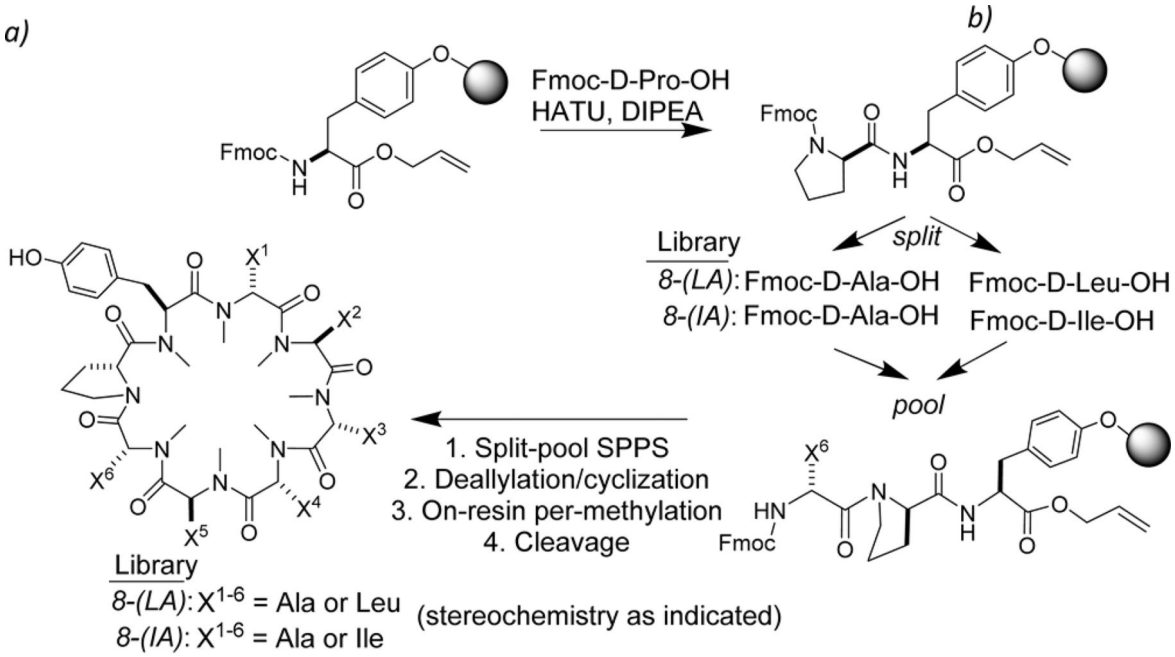

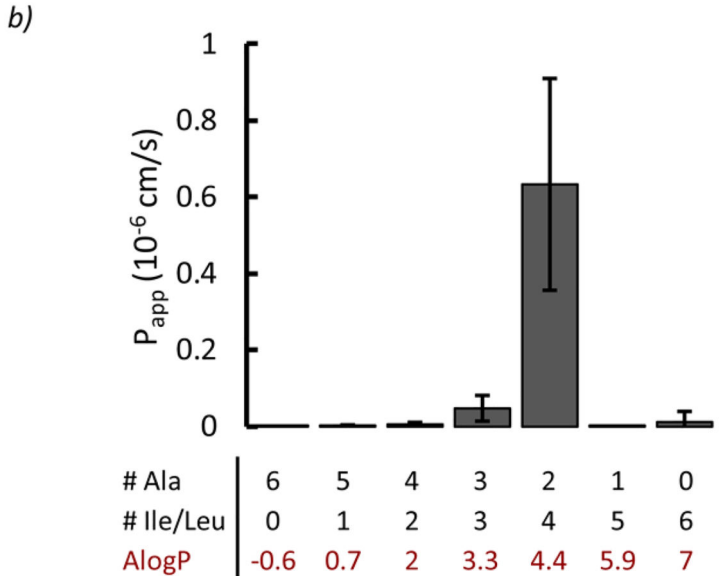

Figure 1.

Octapeptide split pool library. (a) Split-pool synthetic scheme for permethylated Ala scan library. All library members contained a Tyr and Pro residue, and the remaining six positions were Ala, Leu, or Ile. (b) PAMPA permeability of Ala scan library for each unique composition. Di-Ala substitution was the dominantly permeable species in Leu- and Ile-containing library subpools.

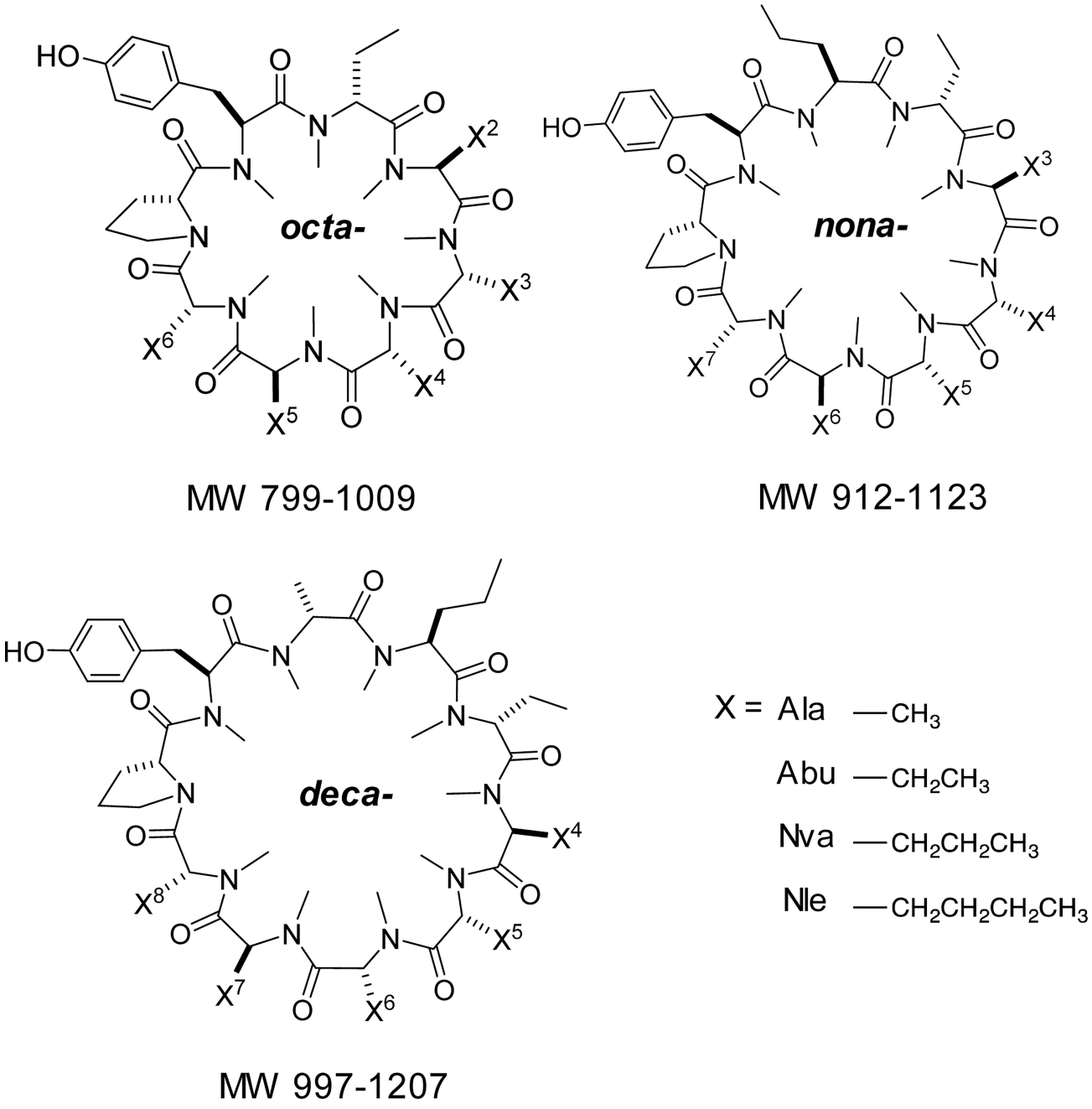

Figure 2.
Lipophilicity scanning library.

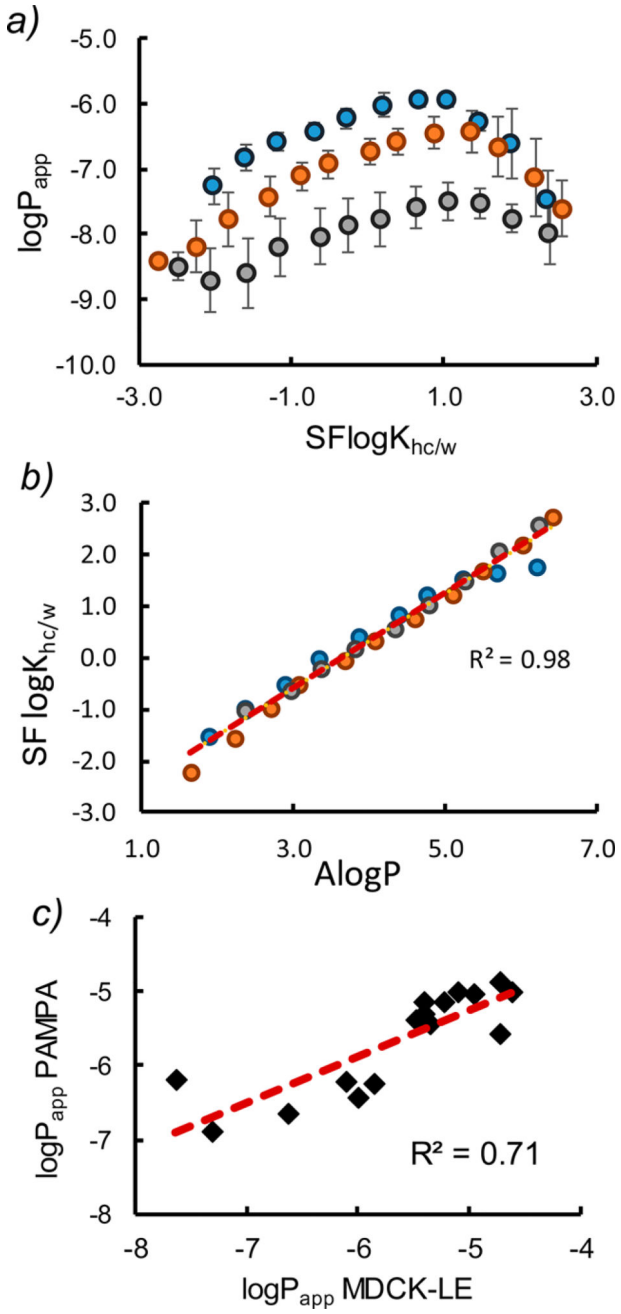

Figure 3.

Variable ring size lipophilicity scanning library. All plots include octa- (blue), nona- (orange), and decapeptides (gray). (a) LogP_{app} vs SFlog$K_{hc/w}$ should be a linear relationship (eq 1), and we observe deviation from linearity in each system at log$K_{hc/w}$ > 1. (b) Experimental 1,9-decadiene partition coefficients (SFlog$K_{hc/w}$) vs *A*log*P*. The linear regression (broken red line) was used to extrapolate values outside the detection limits. (c) LogP_{app} of PAMPA vs MDCK-LE for individual compounds. The linear shape of the data suggests that the PAMPA assay is correlated with the more biologically relevant cell-based

assay. The trends of individual compounds were in agreement with those observed in the mixtures (Table S1).

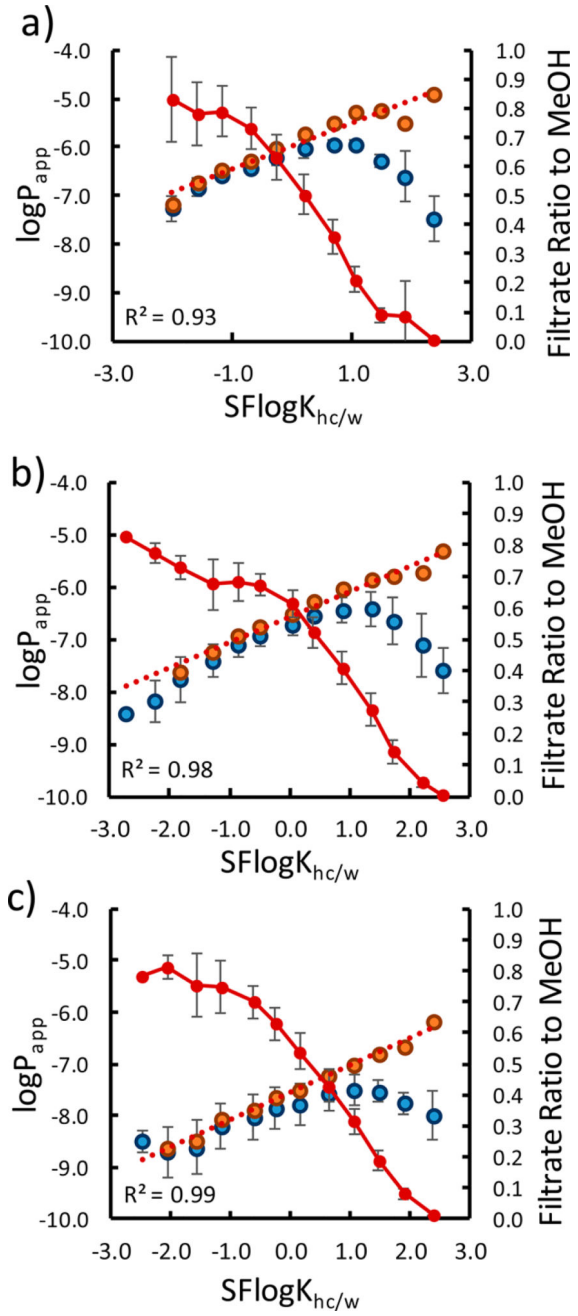

Figure 4.

Solubility-adjusted intrinsic permeabilities. Filtration solubility (unbroken red lines) and logP_{app} for the (a) octa-, (b) nona-, and (c) decapeptides (Figure 2) (blue markers). Solubility-adjusted P_0 values were obtained by dividing the P_{app} by the relative solubility in MeOH for each point (orange markers). The linearity of P_0 and $K_{hc/w}$ is indicated by a linear fit of the solubility-adjusted values (red broken lines).

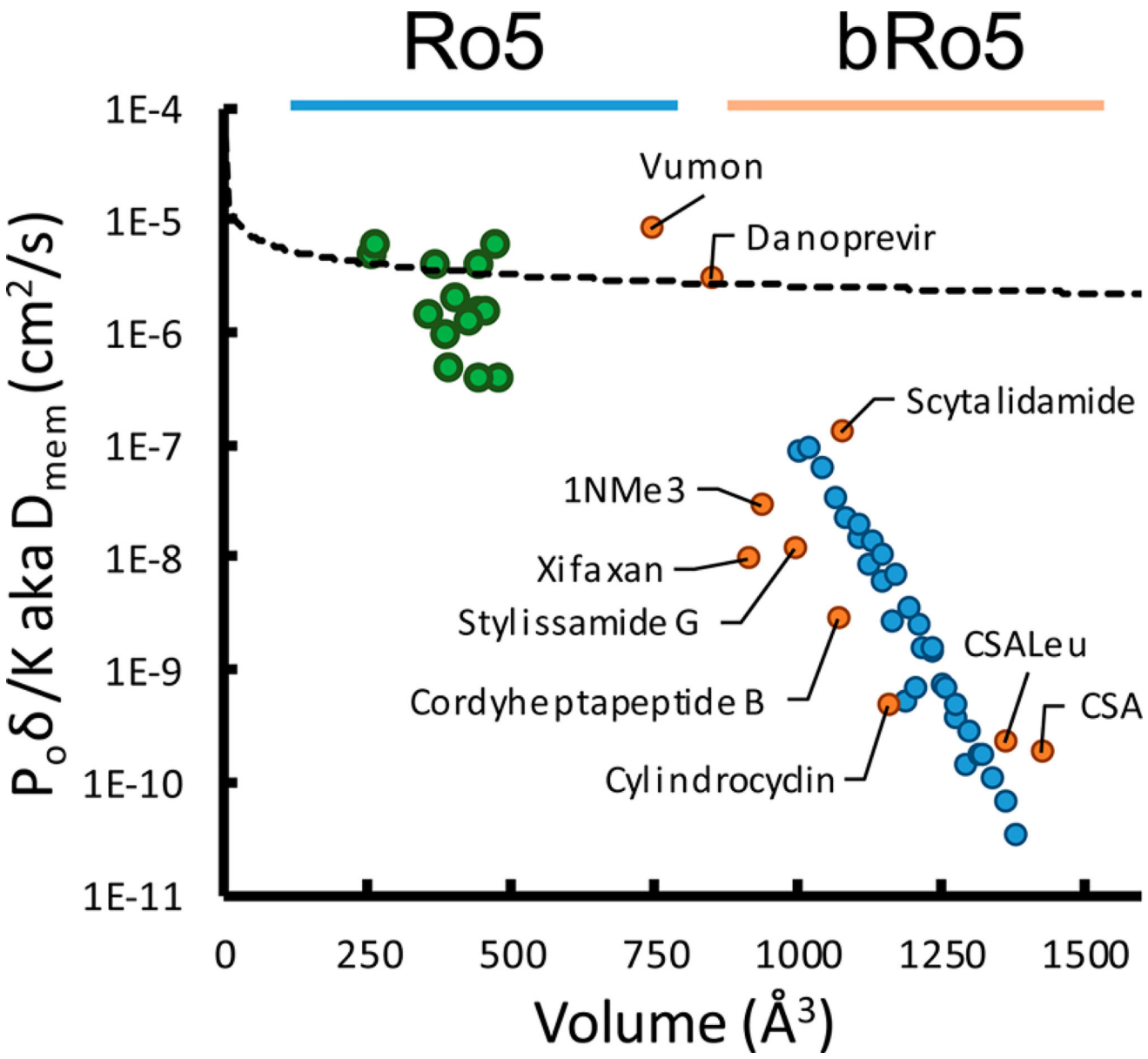

Figure 5.

Membrane diffusion vs molecular volume. Diffusion was determined by eq 4 using experimental values of P_0 and $K_{hc/w}$. The volume was calculated from a 2D structure using a parametrized method. Small Ro5 molecules (green points) roughly follow an exponential trend, whereas the bRo5 lipophilicity scanning library members (Figure 2) (blue points) are subject to a much steeper size penalty. A selection of unrelated synthetic and natural products was subjected to the same analysis to ensure the trends are general (orange points).

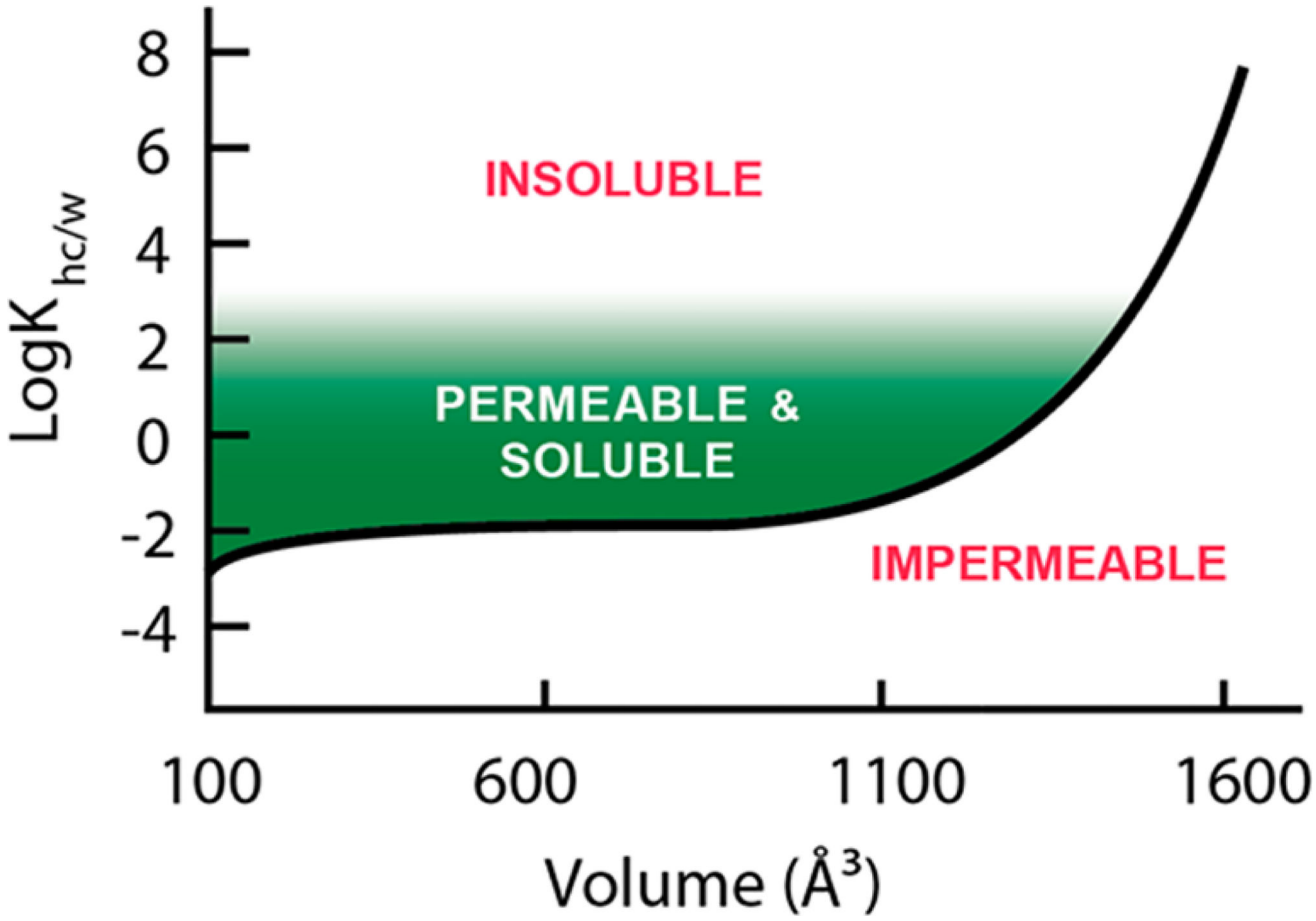

Figure 6.

Property space for passive permeability constrained by polarity, solubility, and molecular volume. The black line represents the lipophilicity required ($\log K_{mem}$) to achieve a permeability of 1×10^{-6} cm/sec for a given volume. The required lipophilicity to overcome the molecular size penalty we observe places an operational limit on molecular volume ~1500 $Å^3$ (~MW 1200).